Mission Replanning for Multiple Agile Earth Observation Satellites Based on Cloud Coverage Forecasting

Yi Gu, Chao Han, Yuhan Chen, and Wei W. Xing

***Abstract*—Recent decades have witnessed a tremendous growth in the number of Earth observation satellites (EOSs), which presents a huge challenge for mission planning. For the EOSs with optical sensors particularly, the observation mission is significantly influenced by the uncertainty of cloud coverage, which has been identified as the most dominant factor for the invalidation of remote sensing images. To overcome this uncertainty, uncertainty programming methods, namely, chance constraint programming (CCP), stochastic expectation model, and robust optimization, are put forth. Despite their success, these approaches are limited in that they simplified the complex cloud coverage uncertainty, which may be different from the true cloud conditions, and they did not take the true cloud information into consideration. Motivated by these recent trends toward Big Data of satellite cloud images and machine learning for spatiotemporal prediction, this article explores a dynamic replanning scheme for multiple EOSs based on cloud forecasting. Specifically, we propose a new approach mainly in the following three steps: first, proactive scheduling based on a CCP is implemented and uploaded via ground control; second, cloud forecasting can be continuously conducted relying on the predictive recurrent neural network and the latest satellite cloud image; and third, mission replanning can be conducted according to the initial schedule and relatively accurate cloud information. Simulation results show that the cloud forecasting method is effective, and the replanning approach presents highly efficient and accurate scheduling results.**

***Index Terms*—Agile Earth observation satellite (AEOS), artificial neural network, cloud forecasting, mission replanning, uncertainty programming.**

I. Introduction

THE last decades have seen the rapid increase of Earth observation satellites (EOSs). The EOS, with its space-based advantage not restricted by geographical conditions, could collect images of the Earth's surface by remote sensors. Corresponding image products have been extensively applied for Earth resource exploration, weather forecasting, disaster monitoring, crop survey, and other areas [1]–[3].

Manuscript received August 31, 2021; revised October 11, 2021 and November 23, 2021; accepted December 12, 2021. Date of publication December 15, 2021; date of current version January 5, 2022. *(Corresponding authors: Chao Han and Wei W. Xing)*.

Yi Gu, Chao Han, and Yuhan Chen are with the School of Astronautics, Beihang University, Beijing 100191, China (e-mail: guyi_buaa@buaa.edu.cn; hanchao@buaa.edu.cn; chenyuhan@buaa.edu.cn).

Wei W. Xing is with the School of Integrated Circuit Science and Engineering, Beihang University, Beijing 100191, China (e-mail: wxing@buaa.edu.cn).

Digital Object Identifier 10.1109/JSTARS.2021.3135529

In practical satellite mission planning, uncertainty always exists, which mainly origins from the cloud occlusion, dynamic observation tasks, and the partial failure of the satellite equipment [4], [5]. According to the observation data of the International Satellite Cloud Climatology Project and Moderate Resolution Imaging Spectroradiometer, the overall global cloud fraction is approximately 67% [6], [7], which reveals that cloud occlusion is extremely serious and almost ubiquitous. Compared to cloud coverage uncertainty, the emergency situations of dynamic observation tasks and equipment failure is more occasionally and unpredictable. Therefore, it is necessary for managers to develop urgent tasks according to the emergency situation. A great deal of research has focused on the mission planning for emergency situations [5], [8]–[11], in which assuming that the dynamic tasks have been generated in advance. On the contrary, the predictable characteristic of cloud coverage provides the potential for EOSs to actively avoid clouds during the mission replanning procedure [5].

Cloud occlusion could cause a considerable negative impact on the optical EOSs mission planning because optical sensors equipped on satellites cannot penetrate clouds for imaging [12]. The statistical data provided by the Union of Concerned Scientists reveal that there were 954 EOSs orbiting the Earth on May 1, 2021 [13], where the number of the optical EOS is 414, accounted for the largest proportion of the EOS. Ju *et al.* [14] reported that about 35% of the images collected by the Landsat-7 sensors were blocked by cloudiness. Beaumet *et al.* [12] pointed out that roughly 80% of the Earth observation of SPOT satellite failed due to cloud occlusion. He *et al.* [15] also reported that nearly 60% of Earth observation images would be trashed owing to excessive cloud covers. The aforementioned studies have assessed the effect of cloud cover and demonstrated the necessity of considering the cloud coverage uncertainty in the EOS mission planning. However, there exist two difficulties in this problem. A real-time and accurate cloud forecasting method is required as a fundamental support. If the result of cloud forecasting deviates seriously from the real situation, the predicted cloud information would mislead the replanning procedure; in the meanwhile, the predicted cloud information would be antiquated if accurate cloud forecasting is delayed, leaving no time for conducting replanning and attitude maneuver operations. Besides, a practical-oriented replanning algorithm framework brings another difficulty to this study, which should

brilliantly combine the cloud forecasting method and rapid mission replanning.

Therefore, the main goal of this study is to investigate the mission planning problem of multiple EOSs based on cloud coverage forecasting. In line with [16], proactive mission planning for multiple agile EOSs (AEOSs) based on the CCP model has been initially implemented. Subsequently, the true cloud information is introduced to the mission planning framework, which could help train the cloud forecasting model and evaluate the result of mission planning. The predictive recurrent neural network (PredRNN) [17] is then adopted to perform accurate cloud forecasting to support the replanning procedure. A rolling horizon-based replanning algorithm (RHRA) based on a rapid insertion strategy is proposed to solve the mission replanning problem effectively.

The main contributions of this study are as follows.

1) To the best of our knowledge, this is the first work to substantially enhance the EOSs mission replanning by harnessing the state-of-the-art deep learning-based cloud forecasting technique. Based on the visibility conditions provided by the predicted cloud information, the effect of mission planning can be significantly improved. The superiority of the proposed method is validated by experiments with comparison to the classic uncertain mission planning method specifically for cloud uncertainty.
2) We present a novel replanning algorithm RHRA, which combines a rapid insertion method and an interval shrinking-based moving strategy to efficiently address the rolling constrained optimization problem induced by combining cloud forecasting and mission replanning. The efficiency and effectiveness of the RHRA are demonstrated with extensive experiments in comparison to other heuristic methods.

The rest of this article is organized as follows. Section II describes a review of the previous studies of satellite mission planning and cloud forecasting. In Section III, the overall algorithm framework and the proactive mission planning model are described. Section IV begins with introducing a deep learning-based cloud forecasting model and looks at the detailed replanning method. In Section V, a series of experiments are conducted to verify the effectiveness of the cloud forecasting and replanning algorithm. Finally, Section VI concludes this article.

II. Literature Review

A. EOS Mission Planning Under Cloud Coverage Uncertainty

Up to now, several researchers have attempted to solve the EOS mission planning problem under cloud coverage uncertainty. We classified the EOS scheduling into the conventional EOS (CEOS) and AEOS mission planning problems in Table I. The main difference between the CEOS and AEOS is the attitude maneuverability [18]. The CEOS has only roll maneuverability, whereas the AEOS is capable of the maneuver of roll, pitch, and yaw axes simultaneously, which will introduce notorious difficulty in AEOS mission planning [19], [20].

TABLE I
Overview of EOS Mission Planning Model Considering Cloud Coverage Uncertainty

Model	The type of EOS	
	Coventional EOS	Agile EOS
Stochastic expectation model	Heuristic [21], B&P [22]	–
Chance constraint programming	B&C [23]	Heuristic [16]
Mixed-integer programming	Commercial solver [24]	Commercial solver [25]
Robust optimization model	Heuristic [26], [27]	Heuristic [28]

As shown in Table I, the mathematical models proposed for mission planning under cloud coverage uncertainty can be summarized as four categories. Liao *et al*. [21] described the uncertain cloud coverage as stochastic events and constructed a model containing the objective of maximizing the expected number of accomplished tasks. Wang *et al*. [22] formulated a stochastic expectation model for CEOS scheduling problems under the impact of the cloud. The profit of a target is simplified depicted as a 0–1 distribution model corresponding to be observed successfully or not under the cloud coverage uncertainty. A branch-and-price (B&P) algorithm including a Dantzig–Wolfe decomposition was proposed to solve the problem efficiently. Though the stochastic expectation model is suitable for the EOS mission planning problem under cloud coverage uncertainty, it lacks the ability to assess the risks of mission planning results. To overcome this shortcoming, a chance constraint programming (CCP) model was introduced to the uncertain CEOS mission planning problem [23]. A parameter indicating the confidence level can be chosen according to the risk control standard in order to reduce the risk of mission planning results. Considering the complexity of the CCP model, a sample approximation method was adopted to transfer the CCP model into the mixed-integer programming (MIP) model. A branch-and-cut (B&C) algorithm was proposed subsequently to solve the converted MIP model. Han *et al*. [16] popularized the CCP model into the more difficult AEOS mission planning problem under cloud coverage uncertainty. Relying on the concept of time slack, an optimization subproblem was established to determine the start time for each observation. Subsequently, an improved simulated annealing-based heuristic consisting of two stages was proposed to solve the problem efficiently.

In line with [23], Xiao *et al*. [24] formulated the cloud coverage for observations as stochastic events with 0–1 distribution. Besides, the confidence level in [23] was maintained to constrain the probability of a successful observation being not less than a minimum threshold. Multiple observations for a target were allowed and the weighted probability of successful observation was established in [24]. An MIP model was later developed for the multiple satellite observation and data-downlink scheduling problem, and a commercial solver was utilized to solve the problem. Valicka *et al*. [25] established several stochastic MIP models for AEOS scheduling to maximize the expected collection quality across a set of sample scenarios representing the cloud coverage uncertainty. The commercial MIP solver CPLEX was used to solve the proposed models and provably optimal or near-optimal schedules can be obtained. However, the engineering constraints of the AEOS were not considered in Valicka's model, which would result in difficulties in application.

The expectation model [22] and the CCP model [23] hold the assumption that one task can only be observed on a single orbit while scheduling one task on several orbits would improve the probability of successful observation. Wang *et al*. [26] established a nonlinear robust mathematical model that could schedule each task on different orbits and proposed three heuristics to solve the large-scale problems. On the basis of the concept of the budgeted uncertainty set, Wang *et al*. [27] provided a robust formulation of the CEOS scheduling problem. The observation profit under cloud coverage uncertainty varies in a bounded profit range discretely, which could ensure an observation image partly covered by the cloud can be awarded. A column-generation-based heuristic was developed to obtain a high-quality feasible solution. Subsequently, Wang *et al*. [28] extended the robust formulation to the AEOS scheduling problem and designed a hybrid heuristic including column generation and simulated annealing to solve the problem.

However, for all of the aforementioned reviewed studies, three defects still exist, which we will now address. First, the complex cloud coverage uncertainty has been simplified, which may be different from the true cloud conditions. The cloud coverage uncertainty model based on 0–1 distribution has been widely used in the expectation and CCP models. This modeling method adopts a simplified observation profit model, no profit assigned under partial cloud cover, which is relatively different from the actual benefit. The robust formulations based on the budgeted uncertainty set [27], [28] could award the images partially obscured by clouds. Nevertheless, only one deviation observation profit has been added considering the computational complexity of the model. Second, the true cloud information has not been utilized in the aforementioned literature. He *et al*. [5] proposed a hierarchical scheduling framework for agile optical satellites, assuming that the dynamic real-time cloud information has been provided. Unfortunately, cloud information has also not been adopted. However, due to the absence of cloud information, the multiple AEOSs mission replanning problem under cloud coverage uncertainty has not been especially studied. Wang *et al*. [29] proposed a reactive scheduling model and algorithm for multiple CEOSs with cloud cover uncertainty, while not applicable for the AEOS mission planning problem owing to the greater attitude maneuverability of the AEOS.

B. Cloud Forecasting Method

When the observation target is blocked by cloud, not only the imaging quality is greatly affected, but the imaging observation of the target will consume resources such as observation time window, satellite storage space, and energy, thereby reducing the observation opportunities for other targets. Therefore, cloud forecasting performs a significant role in EOSs mission planning.

To date, several methods have been adopted to solve the cloud forecasting problem, mainly including numerical weather prediction (NWP) [30], [31] and optical flow method [31]–[34]. Kurzrock *et al*. [30] reviewed the literature for short-term cloud forecasting using the NWP method and pointed that the cloud forecast performance in the first 12–24 h would be strongly influenced by the initial information. Shi *et al*. [35] pointed out that the NWP model is more suitable for long-term forecasting when studying the problem of the precipitation nowcasting problem. Roussel *et al*. [31] reported that the NWP model is computationally intensive and often takes several hours to get the forecasting results. In the light of [31], [36], and[37], the NWP method often consumes several hours to obtain the forecasting results and is not suitable for short-term forecasting, which is difficult to be merged into the replanning framework.

Relying on the cloud motion vector extraction technique, Roussel developed a short-term cloud forecasting method to predict the cloud coverage in the next 6 h. The experimental results show that the proposed method outperforms the NWP in the first 3.5 h. Cros *et al*. [32] proposed correlation phase and optical flow methods to perform cloud forecasting on the six-day image dataset of Meteosat-10. By comparing the predicted cloud image and the true image within 15 min to 4 h, the optical flow method outperforms other methods with satisfactory computing performance. Overall, the optical flow method can be applied for short-term forecasting but abandoning using enormous historical data information. Shi *et al*. [36] proposed the convolutional LSTM (ConvLSTM) and demonstrated that ConvLSTM outperforms the optical flow method in precipitation nowcasting. Unfortunately, the deep learning method for the spatiotemporal sequence prediction that emerged recently [38] has not been adopted in cloud forecasting. ConvLSTM was further improved to build a PredRNN [17], which is utilized to conduct cloud forecasting in our study.

III. Proactive Mission Planning Method

This section starts with an overview of the primary structure of the proactive-and-reactive algorithm, followed by the proactive mission planning method.

A. Algorithm Framework

The primary framework of the proactive-and-reactive mission planning algorithm is summarized in Fig. 1. First, proactive mission planning is performed for the AEOSs scheduling problem under cloud coverage uncertainty, and the model will be introduced later in this section. With the help of the latest satellite cloud images and deep learning methods, cloud forecasting can be rapidly conducted to generate the predicted cloud information. Subsequently, the profit of each task would be updated relying on the cloud forecasting information, and the replanning horizon can be determined according to the length of time for the short-term cloud forecasting. The proposed RHRA would be implemented for each replanning horizon. During the current horizon, tasks that are severely obscured by the cloud will be removed and the available tasks for the same target will be trying to insert in the order of decreasing profit. Moreover, other available tasks on each orbit will also be arranged to observe in the same insertion way to make full use of observation resources. With the time step in, cloud forecasting would be carried out periodically, while the RHRA would improve the mission planning result steadily. If the stopping criterion is met, the final solution can be output, and then, the whole observation

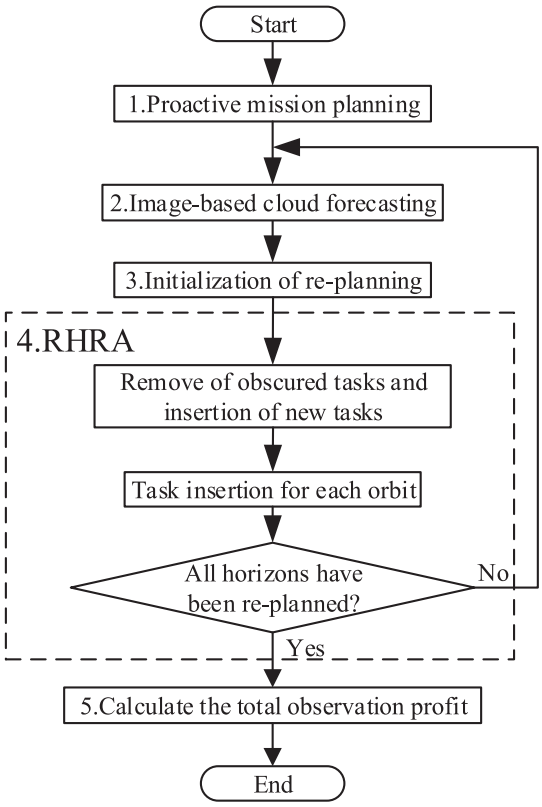

Fig. 1. Structure of the proactive-and-reactive mission planning method.

profit will be calculated. The detailed implementation of each step will be illustrated in the following subsections.

B. Assumptions

This study focuses on solving the mission replanning problem of multiple AEOSs based on cloud forecasting. Thus, the following assumptions and simplifications can be made in order to simply the problem.

1) This study considers the point target exclusively because the polygon target can be decomposed into multiple point targets in line with the field of view of the satellite payload. A point target can be observed in one imaging of satellite and further division of point targets is not considered.
2) At most one observation mission can be conducted by each satellite at one time.
3) Each target cannot be observed more than once owing to the fact that observation resources are relatively limited.
4) Supposing that there are enough ground stations and relay satellites in the scenario, regardless of the data downlink and instruction upload constraints.

C. Notations

In line with [16] and [23], we adopt the CCP model to implement proactive uncertain mission planning. Some notations in this study are summarized in Table II. Let T and O be the set of tasks and orbits, respectively. The set O contains all orbital cycles of satellites in the order of the orbital epoch. A sample approximation method [39] is adopted to solve the chance constraint and W indicates the set of sample scenarios. For each task $i \in T$, od_i denotes the observation duration and ω_i represents the observation profit. If task i can be observed on the orbit k, binary variable b_{ik} is set as 1, otherwise $b_{ik} = 0$. Each orbit $k \in O$ is defined with a memory capacity M_k, an energy capacity E_k, a memory consumption m_k^o and an energy cost e_k^o for unit time observation, and an energy consumption e_k^t for unit angle of attitude transformation. Time intervals $[OS_{ik}, OE_{ik}]$ and $[VS_{ik}, VE_{ik}]$, respectively, denote the observation time window and visible time window of task i on orbit k.

TABLE II
NOTATIONS

Sets	
T	Set of observation tasks, $T = \{1, ..., \|T\|\}$ and $\|T\|$ is the task set size
O	Set of orbits, $O = \{1, ..., \|O\|\}$ and $\|O\|$ is the orbit set size
W	Set of sample scenarios, $W = \{w_1, ..., w_{\|W\|}\}$ and $\|W\|$ is the sample size
Indices	
i, j	Task index, $i, j \in T \cup \{0, \|T\|+1\}$, in which $0, \|T\|+1$ are dummy tasks
k	Orbit index, $k \in O$
l	Sample scenario index, $l \in \{1, ..., \|W\|\}$
Parameters	
od_i	The observation duration of task i, $i \in T$
ω_i	Observation profit of task $i, i \in T$
b_{ik}	$b_{ik} = 1$ if task i can be observed on orbit k, otherwise $b_{ik} = 0$, $i \in T, k \in O$
M_k, E_k	Memory and energy capacity on orbit k, $k \in O$
m_k^o, e_k^o	Memory and energy consumption for unit time of observation on orbit k
e_k^t	Energy consumption for each unit angle of attitude transformation on orbit k
$[OS_{ik}, OE_{ik}]$	Observation time window of task i on orbit k, $i \in T, k \in O$
$[VS_{ik}, VE_{ik}]$	Visible time window of task i on orbit k, $i \in T, k \in O$
se_{ij}^k	Energy consumption in the transformation from i to j on orbit k. $se_{ij}^k = 0$ if j is a dummy task, $i \in T, j \in T \cup \{\|T\|+1\}$, $k \in O$
st_{ij}^k	Attitude transformation time between tasks i and j on orbit k, $i, j \in T, k \in O$
w_l	A scenario, $w_l \in W$
Decision variables	
x_{ik}	Binary decision variable. $x_{ik} = 1$ if task i is scheduled to be observed on orbit k, otherwise $x_{ik} = 0$, $i \in T, k \in O$
TP_{ik}	Continuous decision variable within $[0, 1]$. TP_{ik} is associated to the observation start time for task i on orbit k, $i \in T, k \in O$

After observing one task, the AEOS requires an attitude transformation operation to accomplish the next task. The energy consumed during the transformation from task i to j on orbit k can be formulated as

$$se_{ij}^k = \left(|\theta_{ik}^{\text{Pitch}} - \theta_{jk}^{\text{Pitch}}| + |\theta_{ik}^{\text{Roll}} - \theta_{jk}^{\text{Roll}}|\right) \cdot e_k^t \tag{1}$$

where $\theta_{ik}^{\text{Pitch}}$ and $\theta_{ik}^{\text{Roll}}$ denote the pitch and roll angles for observing task i, respectively.

Let Δg be the total angle change during the transformation, that is $\Delta g = |\theta_{ik}^{\text{Pitch}} - \theta_{jk}^{\text{Pitch}}| + |\theta_{ik}^{\text{Roll}} - \theta_{jk}^{\text{Roll}}|$. The attitude transformation time including an attitude stabilization procedure can

be indicated as st_{ij}^k, which is described as

$$st_{ij}^k = \max\left(|\theta_{ik}^{\text{Pitch}} - \theta_{jk}^{\text{Pitch}}|/v_k^{\text{Pitch}}\ |\theta_{ik}^{\text{Roll}} - \theta_{jk}^{\text{Roll}}|/v_k^{\text{Roll}}\right) + \begin{cases} 5 & \Delta g \le 15^\circ \\ 10 & 15^\circ < \Delta g \le 40^\circ \\ 15 & 40^\circ < \Delta g \le 60^\circ \end{cases} \quad (2)$$

where v_k^{Pitch} and v_k^{Roll} represent the attitude maneuvering angle velocity of pitch and roll axes, respectively.

The binary decision variable x_{ik} represents whether task i would be arranged to be observed on orbit k. TP_{ik} is a continuous decision variable within [0, 1], which can be formulated as follows:

$$OS_{ik} = TP_{ik} \cdot (VE_{ik} - \text{od}_i - VS_{ik}) + VS_{ik} \quad (3)$$

$$OE_{ik} = OS_{ik} + \text{od}_i. \quad (4)$$

Taking the cloud uncertainty into account, the cloud occlusion for each observation is formulated as a stochastic event, denoted by 0–1 random variable $\lambda_{ik}, i \in T, k \in O$. Binary variable λ_{ik} represent whether task i on the orbit k is occluded by cloud or not. The probability that task i can be successfully observed on orbit k is denoted as p_{ik}. Then, we can obtain that $p\{\lambda_{ik} = 1\} = p_{ik}$ and $p\{\lambda_{ik} = 0\} = 1 - p_{ik}$.

D. CCP Model for AEOS Mission Planning

With the parameters described previously, the CCP model of the multi-AEOS mission planning problem can be constructed as

$$\max \quad f \quad (5)$$

subject to

$$P\left\{\sum_{i\in T}\sum_{k\in O}\omega_i \cdot \lambda_{ik} \cdot x_{ik} \ge f\right\} \ge 1 - \alpha \quad (6)$$

$$\sum_{k\in O} x_{ik} \le 1 \qquad \forall i \in T \quad (7)$$

$$x_{ik} \le b_{ik} \qquad \forall i \in T, k \in O \quad (8)$$

$$\sum_{i\in T} x_{ik} \cdot od_i \cdot m_k^o \le M_k \qquad \forall k \in O \quad (9)$$

$$\sum_{i\in T} x_{ik}\left(se_{ij}^k + od_i \cdot e_k^o\right) \le E_k$$

$$j \text{ is the successor task of } i \text{ on orbit } k \qquad \forall k \in O \quad (10)$$

$$\{x_{ik} + x_{jk} \le 1 | \text{if } i \text{ is the pre-task of } j \text{ on orbit } k \text{ and } OE_{ik} + st_{ij}^k > OS_{jk}\} \qquad \forall i, j \in T, k \in O \quad (11)$$

$$x_{ik} \in \{0, 1\} \qquad \forall i \in T, k \in O. \quad (12)$$

The objective function (5) is to maximize the variable f, which is constrained by the chance constraint (6), where $(1 - \alpha)$ indicates the predefined confidence level. The chance constraint (6) denotes that the probability that the observation profit under cloud coverage uncertainty should be at least f, is not less than the confidence level $1 - \alpha$. Constraints (7) and (8) indicate that each task cannot be observed repeatedly and should meet the visibility condition. Memory constraints (9) and energy constraints (10) represent the resource constraints of each orbit. Constraints (11) indicate that when the sum of the observation end time of task i and the attitude transformation time st_{ij}^k is greater than the observation start time of task j, adjacent tasks i and j cannot be observed simultaneously.

Owing to the difficulty in calculating the probability in the chance constraint (6), a sample approximation method [39] is introduced to determine the observation profit approximately. The Monte Carlo simulation [40] is adopted to create a set of sample scenarios $\{w_1, \ldots, w_{|W|}\}$ for the random variable $\lambda_{ik}, i \in T, k \in O$. The basic idea of sample approximation reformulation is to solve the problem and obtain a solution, which is infeasible for at most $|W| \cdot \epsilon$ scenarios. Then, the confidence level of the solution for the sample approximation problem will be at least $(1 - \epsilon)$. Let $y_l, l \in \{1, \ldots, |W|\}$ be binary variables, $y_l = 1$ if current solution is infeasible in scenario $w_l \in W$, otherwise $y_l = 0$. The chance constraint (6) can then be reformulated as follows.

$$\sum_{i\in T}\sum_{k\in O}\omega_i \cdot \lambda_{ik}^l \cdot x_{ik} \ge -y_l \cdot Z + f \qquad \forall w_l \in W \quad (13)$$

$$\sum_{w_l \in W} y_l \le |W| \cdot \epsilon \quad (14)$$

$$y_l \in \{0, 1\} \qquad \forall w_l \in W. \quad (15)$$

In constraints (13), λ_{ik}^l represents the sample value of λ_{ik} under scenario w_l and Z denotes a large number. Constraints (13) indicate that the objective function f should not be greater than the observation profit for scenario w_l when $y_l = 0$. The number of scenarios where the solution is infeasible, at most be $|W| \cdot \epsilon$, is restricted by constraints (14). The infeasible solution where y_l equals 1 means that the observation profit $\sum_{i\in T}\sum_{k\in O}\omega_i \cdot \lambda_{ik}^l \cdot x_{ik}$ could be less than f. Thus, the reformulation of the original CCP model is: maximize f, subject to constraints (7)–(12) and (13)–(15).

The value of the sample size $|W|$ is inherited from [16], and the used parameters are set as: $1 - \alpha = 0.90, 1 - \epsilon = 0.99$, and $Z = 10^6$. The detailed algorithm for solving the proactive mission planning problem can be found in [16]. The proactive mission planning result is the basis of the replanning procedure in this research. In previous studies [16], [23], the uncertain mission planning results have not been evaluated according to the true cloud information, which has prompted this research to introduce the cloud data and make a comparison between the proactive and reactive mission planning results.

IV. Mission Replanning Based on Cloud Forecasting

To clearly express the proposed method, this section begins with the introduction of the cloud forecasting method, and then, describes the replanning method exhaustively.

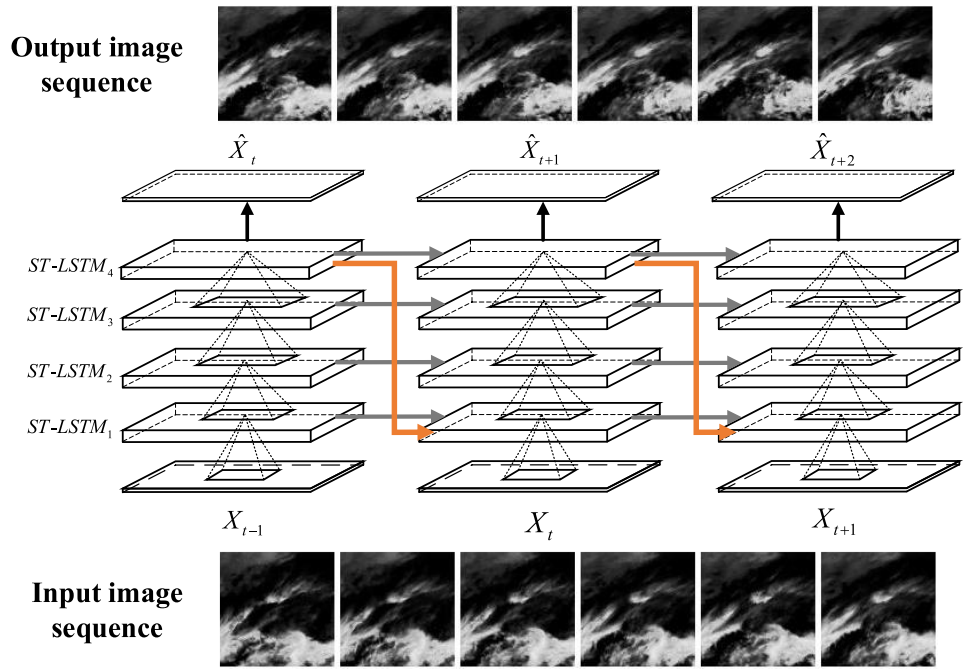

Fig. 2. PredRNN framework for short-term cloud forecasting.

A. *Deep-Learning-Based Cloud Forecasting Model*

To perform an effective mission replanning, valid cloud forecasting should be conducted at first. The NWP method fails to make fast and reliable short-term forecasts, and we adopt PredRNN to conduct the cloud forecasting. The traditional LSTM focuses more on modeling temporal variations, while a new spatiotemporal LSTM (ST-LSTM) unit is presented in PredRNN. The LSTM unit only contains a standard temporal memory, while the ST-LSTM also records and utilizes the spatiotemporal memory for predictive output, which is detailed in [17]. The spatiotemporal memory is memorized in a unified memory pool and could be shared with all ST-LSTMs by the PredRNN network. As shown in Fig. 2, stacked ST-LSTMs could extract abstract features layer-by-layer and conduct predictions by mapping them back to the gray value space. The gray arrows denote the temporal memory transfer across states in the traditional LSTM. The orange zigzag arrows represent the transition path of the spatiotemporal memory, which achieves the transmission of memory vertically across layers. In this way, the PredRNN can take into account both spatial and temporal memory and convey it both vertically across layers and horizontally over states.

The FY-2 satellite cloud image is utilized in this study, which can be obtained from the website of the national satellite meteorological center [41]. The background of each image is removed by subtracting the base image. The gray-scale images containing cloud information are then acquired through the brightness extraction method based on the HSV color space [42]. Subsequently, the moving cloud sequence dataset can be generated by arranging a large number of gray-scale images containing time information together. The cloud image dataset consists of optical observations of FY-2 recorded every 30 min, which varies from September 2017 to April 2018. After the cloud extraction, each original image can be transformed to a 300 $\times$ 300 gray-scale image, which represents the cloud distribution of the interest area. Then, the consecutive images are sliced with a 12-frame-wide sliding window and 8000 sequences can be obtained. Thus, each sequence consists of 12 frames, 6 for the input and 6 for forecasting. The total 8000 sequences are divided into a training set of 6400 samples, a valid set of 800 samples, and a test set of 800 samples.

B. *Initialization of Replanning*

In order to execute the replanning algorithm, the predicted cloud information should be adopted for each task to determine the observation profit under cloud coverage. Since intermittent 2-D cloud images of a certain area of the next few hours can be generated, it is necessary to analyze the spatial and temporal characteristics of images. We would neglect the influence of the cloud height because of its huge gap compared to the altitude of the EOS. Generally, the altitude of the EOS can vary from 500 to 1000 km [43], while the cloud base height mainly varies from 60 to 12km [44]. For the sake of fairness, the altitude of the EOS is fixed as 700 km and the cloud base height is set as 10 km for the following analysis. As shown in Fig. 3, the schematic of cloud occlusion when a satellite is observing a target is presented on the left, while the satellite-to-site view geometry is provided on the right. In the subplot (a), the size of the ground point target is set as 50 km$\times$50 km, which is related to the field of view of the satellite payload. Then, the maximum visible elevation angle that can avoid the cloud cover can be calculated as $\beta = \arctan(10/25) \approx 21.801°$. Namely, the cloud above this target would no longer cause an impact if the elevation angle of sight from target to satellite is less than β. The Earth is simplified as a sphere with a diameter of 6400 km in

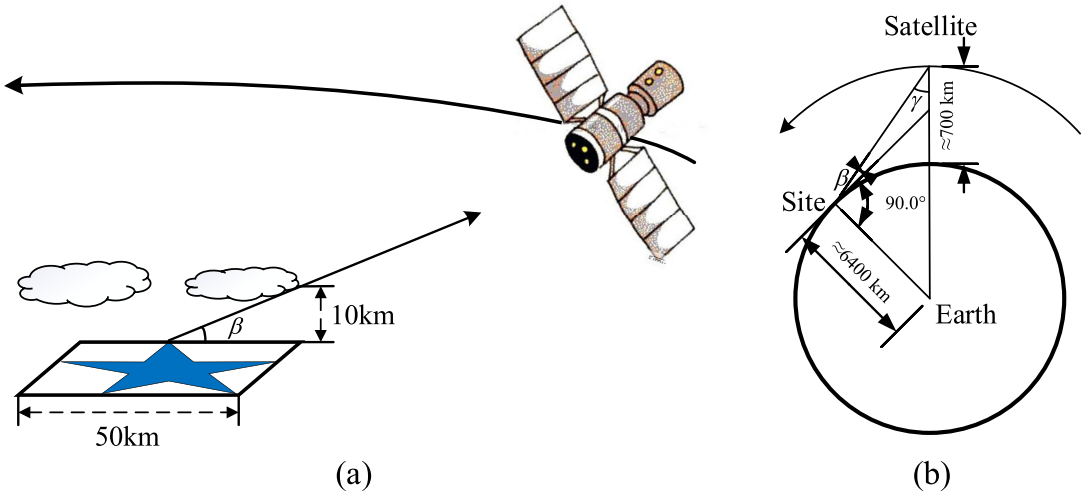

Fig. 3. Schematic of the cloud occlusion and satellite-to-site view geometry.

subplot (b), and γ indicates the satellite pitch angle. According to the law of sines of triangles, we have

$$\frac{6400}{\sin\gamma} = \frac{7100}{\sin(90^\circ + \beta)}. \tag{16}$$

Then, $\gamma \approx 56.818^\circ$ can be obtained. However, it is difficult for an AEOS to own such a strong pitching maneuverability. Meanwhile, the photo captured with a large pitch angle is likely to be useless owing to its poor quality. Note that if the cloud base height is lower than the value set in Fig. 3, these constraints will be more stringent. If there exist clouds above a ground target, therefore, we assume that the partial cloud occlusion is almost inevitable no matter what look angles of the AEOS while imaging the target. The cloud coverage percentage, denoted as δ, is introduced to represent the effect of cloud occlusion. The cloud coverage when observing task i is indicated as δ_i, which can be determined by the predicted cloud information. The cloud images above the concerned area, namely where task i is located, have been predicted at a few specific moments, then the corresponding cloud coverage percentage can be determined. Considering that the cloud coverage will not change drastically during the period of the visible time window, the value of δ_i can be calculated by the linear interpolation of several cloud coverage percentages.

Owing to the difficulty of model solving, the observation profit is simplified as 0–1 mode in the CCP model [23], which does not take the reward of images with partial cloud cover into consideration. The introduction of cloud forecast information makes it possible to consider the partial revenue. As illustrated in Fig. 4, a linear profit model is proposed in order to depict the observation profit under cloud coverage, where δ_0 indicates the cloud coverage threshold. The objective function of the replanning procedure can be described as

$$\max \quad \sum_{i\in T}\sum_{k\in O}(1-\delta_i)\cdot\omega_i\cdot x_{ik}. \tag{17}$$

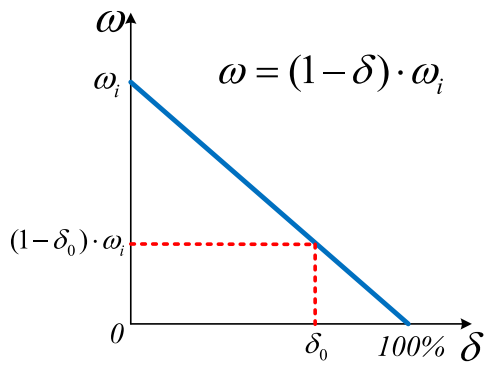

Fig. 4. Linear function for the observation profit of each task under the cloud coverage.

The function (17) is to maximize the total observation profit under the predicted cloud information. Then, the mathematical model of the reactive mission planning is formulated as: maximize objective function (17), and subject to constraints (7)–(12).

C. Rolling Horizon-Based Replanning Algorithm (RHRA)

Previous studies have proved that the AEOS mission planning problem is NP-hard, namely that it is difficult to find the optimal solution within polynomial time [19]. Mission replanning based on the real cloud information is highly required for operating efficiency. Therefore, the RHRA based on the rapid insertion strategy is developed in this article to improve the proactive mission planning result while satisfying engineering constraints.

1) Main Procedure: The rolling horizon (RH) approach consists in dividing the entire time horizon into shorter time intervals according to the length of cloud forecasting. Fig. 5 concisely illustrates the RH-based replanning procedure. The RH approach replans the observation mission every fixed time interval, which is possible because the uncertain cloud coverage can be forecasted relying on the real cloud images arriving periodically. As depicted in Fig. 5, axis $Time$ contains a part

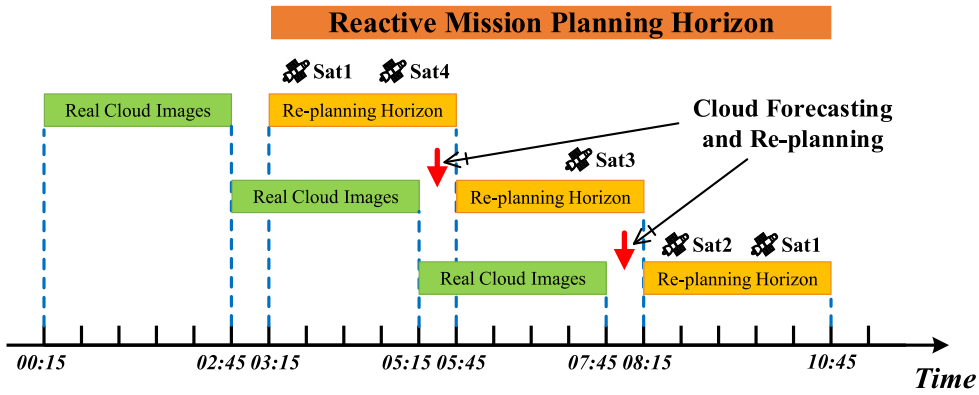

Fig. 5. Schematic of the RH-based replanning procedure.

of the scenario time and the green square indicates the input sequence of real cloud images. The total reactive mission planning horizon is divided into several replanning horizons based on the forecasting time intervals. Satellite icons are located above the replanning horizon, which indicates that mission replanning should be conducted for these satellites owing to the existing visible time windows during this time interval. The red arrow represents the procedure of cloud forecasting and the mission replanning. Considering the algorithm running and data transmission time in engineering applications, the fixed time interval between real images arriving and the replanning horizon is reserved.

Algorithm 1 shows the pseudocode of the framework of the RHRA. Briefly, for each replanning horizon, the current solution S_c is improved to a better one S_p, where the task pool containing the information of missions performs a significant role. $ArrTaskPool$ stores the task information, which has been scheduled for observation, and it will be updated at the end of each replanning horizon. $CurrTaskPool$ contains the task information, which is consistent with S_c in the current replanning horizon. For the current replanning horizon, tasks corresponding to targets that have not been arranged to observe are collected in $AvaTaskPool$, providing alternative resources for task insertion. Meanwhile, $AvaTaskPool$ would be updated immediately when a task is removed or inserted successfully. Besides, the removed task pool $RemTaskPool$ and the substitute task pool $SubTaskPool$ will be initialized in the program. First, we remove the target, which has been observed in $ArrTaskPool$ from the current task pool, as well as tasks related to this target in $AvaTaskPool$. This operation will ensure each task would not be observed redundantly under the condition of scarce resources. If the predicted cloud coverage δ_i exceeds the threshold δ_0, the corresponding task i will be removed from $CurrTaskPool$ to $RemTaskPool$ owing to the encouragement of the higher observation profit. After the removing step, we search the task $j \in AvaTaskPool$ with the same observation target of each task in $RemTaskPool$ and build up the $SubTaskPool$ in descending order of profit. Then, a rapid insertion of task j to the current solution S_c will be conducted. Once inserted successfully, $CurrTaskPool$ and $AvaTaskPool$ will be renewed, as well as out of the loop. Subsequently, we obtain available tasks for each orbit k in the current replanning horizon and make up $AvaTaskPool_k$. Relying on the linear profit model under the predicted cloud information, tasks are attempted to be inserted to S_c in the order of revenue from highest to lowest. The insertion will be successful if constraints (9)–(11) are satisfied. When all horizons within the reactive mission planning have been replanned, the RHRA ends and output the replanning result S_p.

2) Rapid Insertion: Attitude transformation constraints (11) associated with the observation start time are coupled with visible time constraints (8) and resource constraints (9) and (10), which will increase the difficulty and complexity of an insertion procedure enormously. On the one hand, it should be verified that the attitude transformation constraints are satisfied when inserting an unarranged task. The moving forward and backward strategies along the time axis contribute to search a suitable position for the insertion. On the other hand, the energy constraint which is related to the insert position should be checked. Note that this key constraint for the AEOS mission planning has not been taken into consideration in several related studies [18], [45], [46].

The pseudocode of the rapid insert procedure is presented in Algorithm 2. The current solution S_c and the task i to be inserted are required. For the current result S_k on the orbit k where task i locates, a task sequence $\{i_p, i, i_s\}$ is utilized to execute the insertion procedure. As an illustration, notation $\{i, i_s\}$ indicates the continuous task sequence of i and i_s. The real variable $TP_{ik} \in [0, 1]$, denoting the position of observation start time, is initialized as 0.5 and the logical variable $Label$ is set as $False$. To begin the insertion process, it is necessary to determine whether adjacent tasks are empty. Then, the insertion procedure will be on a different track according to the judgment result. Generally, once the attitude transformation constraint is verified, following the check for memory and energy constraints. If the attitude transformation constraint of $\{i, i_s\}$ is violated, we will attempt to move OS_{ik} to an earlier time through decreasing the value of TP_{ik}. Movement operation in the opposite direction would be conducted when the attitude transformation constraint of $\{i_p, i\}$ is violated. A detailed description of the movement can be found in Algorithms 3 and 4.

3) Interval Shrinkage-Based Moving Strategy: For the purpose of stability of the engineering system, the replanning algorithm should change the proactive mission planning result as

Algorithm 1: Procedure of RHRA.

Input:
Current mission planning result S_c, the arranged task pool $ArrTaskPool$, current task pool $CurrTaskPool$, current available task pool $AvaTaskPool$, the removed task pool $RemTaskPool$, the substitute task pool $SubTaskPool$, cloud coverage threshold δ_0 and the predicted cloud coverage δ_i for each task i;

Output:
The re-planning result S_p

while existing the horizon has not been re-planned **do**
  for $i \in CurrTaskPool$ which has been observed in $ArrTaskPool$ **do**
    Remove task i from $CurrTaskPool$ and update $AvaTaskPool$;
  end for
  $RemTaskPool \leftarrow \emptyset$;
  if $i \in CurrTaskPool$ and $\delta_i > \delta_0$ **then**
    Remove task i from $CurrTaskPool$ to $RemTaskPool$;
    Update S_c and $AvaTaskPool$;
  end if
  for $i \in RemTaskPool$ **do**
    $SubTaskPool \leftarrow \emptyset$;
    Search the task $j \in AvaTaskPool$ with the same observation target of i;
    Make up the $SubTaskPool$ in descending order of $(1-\delta_j)\cdot\omega_j$;
    for $j \in SubTaskPool$ and $\delta_j \leq \delta_0$ **do**
      $S_c \leftarrow RapidInsertion(S_c, j)$;
      if $Label$ is $True$ **then**
        $CurrTaskPool \leftarrow j$;
        Update the $AvaTaskPool$;
        break;
      end if
    end for
  end for
  for each orbit k in current replanning horizon **do**
    Make up $AvaTaskPool_k$ in the descending order of profit;
    for $j \in AvaTaskPool_k$ and $\delta_j \leq \delta_0$ **do**
      Execute Steps 15–20;
    end for
  end for
  Update $ArrTaskPool$ according to S_c;
end while
$S_p \leftarrow S_c$

Algorithm 2: RapidInsertion(S_c, i).

Input:
Current mission planning result S_c and task i to be inserted;

Output:
S_c and logical variable $Label$ indicating whether the insertion is successful;

Initialization: $TP_{ik} \leftarrow 0.5$, $Label \leftarrow False$;
Obtain the orbital solution S_k on the same orbit as task i from S_c;
Determine the precursor task i_p and the successor task i_s of task i on current orbit k;
if $i_p = \emptyset$ and $i_s = \emptyset$ **then**
  $Label \leftarrow True$;
else if $i_p = \emptyset$ **then**
  if Constraint (11) of $\{i, i_s\}$ is satisfied **then**
    if Constraints (9) and (10) are satisfied **then**
      $Label \leftarrow True$ and update S_c;
    end if
  else
    $MoveForward(TP_{ik})$;
    if $Label_F$ is $True$ **then**
      Execute Steps 8-10;
    end if
  end if
else if $i_s = \emptyset$ **then**
  if Constraint (11) of $\{i_p, i\}$ is satisfied **then**
    Execute Steps 8–10;
  else
    $MoveBackward(TP_{ik})$;
    if $Label_B$ is $True$ **then**
      Execute Steps 8–10;
    end if
  end if
else
  if Constraints (11) of $\{i_p, i\}$ and $\{i, i_s\}$ are satisfied **then**
    Execute Steps 8–10;
  else if Constraint (11) of $\{i, i_s\}$ is satisfied **then**
    Execute Steps 21–24;
  else if Constraint (11) of $\{i_p, i\}$ is satisfied **then**
    Execute Steps 12–15;
  end if
end if

little as possible [29]. Peng *et al.* [46] proposed an insert procedure for the AEOS scheduling problem with time-dependent profits, which will attempt to move all tasks on the orbit to be inserted for the optimal solution. However, the change of all tasks will cause greater difficulties to operation instruction generation and algorithm robustness during the replanning procedure. An interval shrinkage-based moving strategy specifically for the insertion task, therefore, is proposed in the rapid insertion to ensure stability and rapidity simultaneously.

Algorithm 3 moves the task i to an earlier observation time, which should exceed the observation start time of task i and the observation end time of task i_p. When there remains a time interval between OS_{ik} and $\max(VS_{ik}, OE_{i_pk})$ exceeding 2 s, the observation start time of task i would be set at the middle location. Following the move, the attitude transformation constraint will be checked. The program will jump out of the loop if corresponding constraints are satisfied. Similarly, Algorithm 4

Algorithm 3: MoveForward(TP_{ik}).

Input:
Information of the task i to be inserted, the precursor task i_p and the successor task i_s
Output:
Logical variable $Label_F$ indicating whether the forward moving is successful;

Initialization: $Label_F \leftarrow False$ and calculate OS_{ik} according to (3);
if $i_p = \emptyset$ **then**
  $OE_{i_pk} \leftarrow VS_{ik}$
else
  Calculate OE_{i_pk} according to (4);
end if
while $OS_{ik} - \max(VS_{ik}, OE_{i_pk}) \geq 2$ **do**
  $OS_{ik} = 0.5 * (OS_{ik} + \max(VS_{ik}, OE_{i_pk}))$;
  if $i_p = \emptyset$ **then**
    if Constraint (11) of $\{i, i_s\}$ is satisfied **then**
      $Label_F \leftarrow True$ and break;
    end if
  else
    if Constraints (11) of $\{i_p, i\}$ and $\{i, i_s\}$ are satisfied **then**
      $Label_F \leftarrow True$ and break;
    end if
  end if
end while

Algorithm 4: MoveBackward(TP_{ik}).

Input:
Information of the task i to be inserted, the precursor task i_p and the successor task i_s
Output:
Logical variable $Label_B$ indicating whether the backward moving is successful;

Initialization: $Label_B \leftarrow False$ and calculate OS_{ik} according to (3);
if $i_s = \emptyset$ **then**
  $OS_{i_sk} \leftarrow VE_{ik}$
else
  Calculate OS_{i_sk} according to (3);
end if
while $\min(VE_{ik}, OS_{i_sk}) - OS_{ik} \geq 2$ **do**
  $OS_{ik} = 0.5 * (OS_{ik} + \min(VE_{ik}, OS_{i_sk}))$;
  if $i_s = \emptyset$ **then**
    if Constraint (11) of $\{i_p, i\}$ is satisfied **then**
      $Label_B \leftarrow True$ and break;
    end if
  else
    if Constraints (11) of $\{i_p, i\}$ and $\{i, i_s\}$ are satisfied **then**
      $Label_B \leftarrow True$ and break;
    end if
  end if
end while

will conduct the movement in the opposite direction for the insertion of task i. Finally, a logical variable indicating whether the moving is successful will be output.

V. Computational Experiments

In this section, extensive numerical experiments are conducted to evaluate the proposed model and algorithm. The computational experiments have four goals: verify the accuracy of the cloud forecasting method, evaluate the effectiveness of the proposed replanning algorithm, make a comparison for results with different forecast times, and conduct the sensitivity analysis of parameters ϵ and δ_0.

Since we are the first to solve the AEOS replanning problem, which takes the true cloud information into account, we cannot compare the performance of the proposed RHRA with other approaches diametrically. Therefore, we mainly compare the performance of our algorithm with the proactive mission planning result, as well as the replanning results with other heuristics.

A. Data Generation

The cloud forecasting algorithm is coded in Python based on the PyTorch framework [47]. The proactive-and-reactive mission planning program is implemented in MATLAB. The replanning experiments are conducted on a desktop with Intel Core i74790 K CPU at 4.00 GHz and 16.0 GB of RAM. Without a benchmark dataset for the AEOSs replanning problems, several instances are designed in line with the satellite cloud image data. The interest region within the field of view coverage of FY-2 is predefined in a sea area (9° N-24° N and 126° E-141° E). Then, several scenarios with a different number of observation targets (50, 100, 150, and 200) are randomly generated in the area. The observation profit for each target is uniformly distributed in [0, 10] and ω_i of each task i inherits the profit of the corresponding target. The observation duration for each target is fixed as 10 s. To perform the visibility calculation, the minimum solar altitude angle and the minimum elevation angle for each observation task are set as 0° and 15°, respectively.

TABLE III
Orbital Parameters of the Agile Satellites

ID	a(km)	e	I(°)	Ω (°)	A (°)	M (°)
Sat1	6903.673	0.001655	97.5839	97.8446	50.5083	2.0288
Sat2	6903.730	0.001558	97.5310	95.1761	52.2620	31.4501
Sat3	6909.065	0.000997	97.5840	93.1999	254.4613	155.2256
Sat4	6898.602	0.001460	97.5825	92.3563	276.7332	140.1878

The start time of the scenario is set as 2018/04/18 00:00:00 and the mission horizon is 24 h. The orbital parameters of selected AEOSs in the scenario are shown in Table III, where the column ID represents the name of each satellite, while other columns denote the length of semimajor axis (a), eccentricity (e), inclination (I), right ascension of the ascending node (Ω), the argument of perigee (A), and mean anomaly (M), respectively. The largest roll and pitch degrees of each AEOS are all set as 30°, while the angular velocities v_k^{Pitch} and v_k^{Roll} can be designed

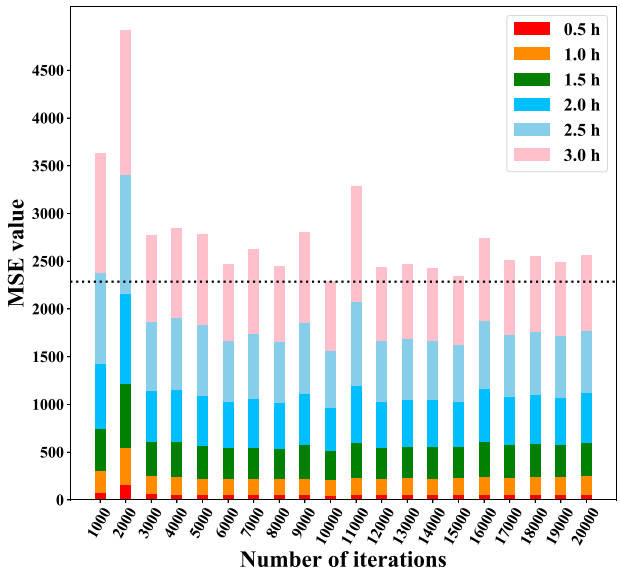

Fig. 6. Schematic of the variation of MSE with the number of training iterations.

as $3^\circ/\text{s}$. The parameters for each orbit $k \in O$ can be defined as: $M_k = 5000$ MB, $E_k = 80$ kJ, $m_k^o = 100$ MB/s, $e_k^o = 500$ J/s, and $e_k^t = 1000$ J/°. Besides, the value of the cloud coverage threshold is initialized as $\delta_0 = 70\%$.

B. Accuracy Analysis of Cloud Forecasting Results

As mentioned in Section IV-A, the forecasting method based on the PredRNN is introduced to conduct cloud forecasting for an arbitrary input image sequence. The effect of each training model is tested on the validation set, where the mean square error (MSE) between the predicted and true images is introduced to conduct the evaluation. The calculation of the MSE can be expressed as

$$\text{MSE} = \frac{1}{N}\sum_{n=1}^{N}\sum_{p=1}^{P}(g_p - \hat{g}_p)^2 \tag{18}$$

where N indicates the number of images used for verification and P denotes the number of pixels in each image. Moreover, g_p represents the true gray value of the pixel p, while $\hat{g}_p$ indicates the predicted one.

Fig. 6 presents the change of the MSE with the number of training at each forecast time step. It is apparent from the length of the bar of different colors that the MSE will become larger as the forecast time increase. This result may be explained by the fact that the short-term forecasts based on real data are more accurate. From the chart, it can be seen that the total MSE achieves the lowest at the epoch of the 10000th iteration of training. Then, the training error would increase sharply at the 11000th iterations, and a possible explanation for this might be overfitting. Therefore, the training model generated by the 10000th iteration is adopted to conduct the cloud forecasting in the following experiment.

To evaluate the performance of the PredRNN, a comparative experiment with the optical flow method [36] has been

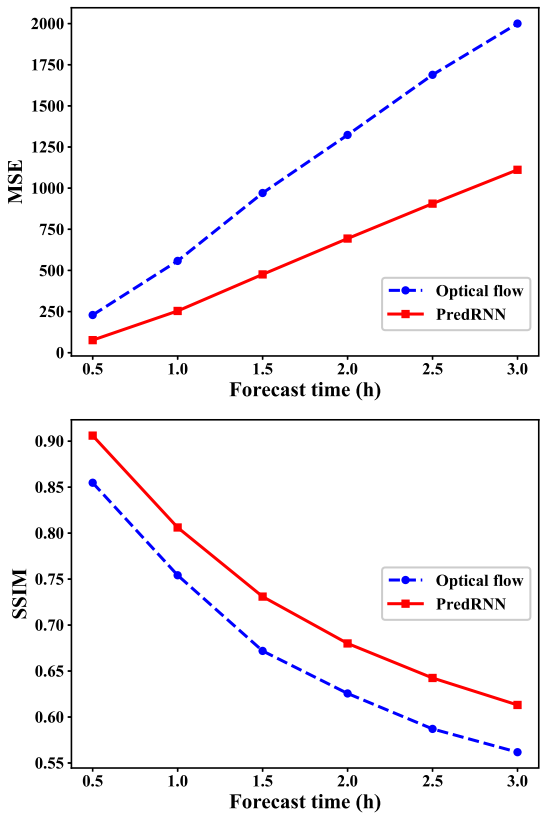

Fig. 7. Comparison of different cloud forecasting methods based on two metrics over time.

conducted. For the optical flow method, we tune the different initialization schemes of the optical flow and use the best scheme, which initialized the flow velocity by the means of the last two flow fields, to report the results. The comparison results are shown in Fig. 7, where the SSIM indicates the structural similarity [48] between the predicted and true image. A lower value of the MSE and a higher value of SSIM represent a better forecasting effect. It is apparent from the figure that the forecast accuracy of both methods will decrease as the forecast time increases. As can be seen from Fig. 7, the performance of the PredRNN is better than the optical flow method. What is interesting is the steady growth of the numerical gap as the forecast time increases, which means a more significant advantage for the PredRNN. The flow vector will be calculated in each step of the forecast by the optical flow method, therefore, longer operation time is also required compared to the PredRNN.

Owing to the fact that the cloud coverage ratio of each task is utilized, we make statistics for the average results of the cloud coverage error E_i to validate the feasibility of the cloud forecasting. The formulation of E_i is as follows:

$$E_i = 100 \times \frac{1}{N}\sum_{n=1}^{N}|\delta_i - \hat{\delta}_i| \qquad \forall i \in T \tag{19}$$

where $\hat{\delta}_i$ represents the cloud coverage percentage of a square area with 100 pixels in the forecast cloud image. The side length of the area is about 50 km, which is principally consistent with the width of the field of view for the payload of each AEOS.

Fig. 8. Average value of cloud coverage error when the forecast time is 3 h.

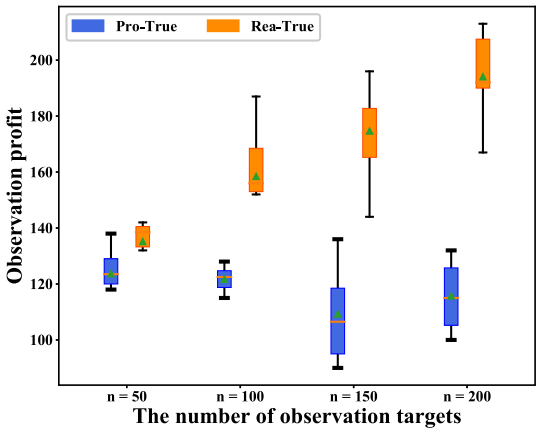

Fig. 9. Comparison of observation profits of proactive-and-reactive mission planning.

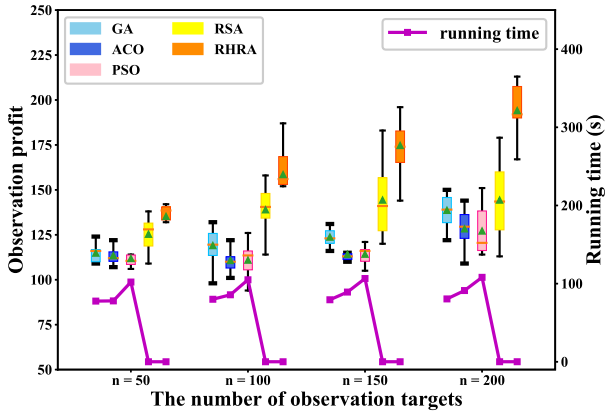

Fig. 10. Comparison experiment results with different algorithms.

As can be seen from Fig. 8, E_i within partial areas when the forecast time equals 3 h is presented by way of the heat map, where the value of the cloud coverage error is displayed on each little square. Note the value of E_i would increase with the forecast time, which means that Fig. 8 illustrates the largest error within the forecast time. We can find that the forecast accuracy

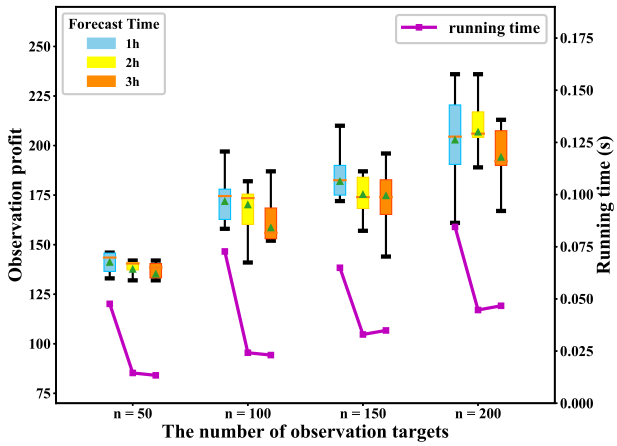

Fig. 11. Comparison of the true observation profit and running time under different forecast times.

owns the characteristics of regional differences, which may be explained by the fact that the degree of cloud cover changes varies in different regions. Data from this Figure show that the percentage of the cloud coverage error at the third-hour forecast is exclusively around 10%. This means the result of cloud forecasting can provide valid guidance for mission replanning.

C. *Effectiveness Verification of the Replanning Algorithm*

To verify the feasibility of the proposed replanning algorithm, comparative experiments between proactive and reactive mission planning have been conducted. As shown in Fig. 9, abbreviations Pro-True and Rea-True represent the observation profit of the proactive and reactive mission planning respectively, which are recalculated by the proposed linear profit model utilizing the true cloud information. For each scenario with a certain number of observation targets, ten runs have been conducted. The average and the median of ten observation profits are denoted as the green triangle symbol and the orange horizontal line, respectively. The box plot represents the distribution of the result, and different colors indicate the observation profit of different circumstances, which can be determined by the legend.

What stands out in the figure is that the average profits of the replanning results are all higher than that of the corresponding proactive mission planning result. These results confirm that the proposed RHRA would improve the proactive mission planning results. Besides, the observation profit of the replanning result would increase as the number of observation targets increases. A similar tendency cannot be observed obviously for the proactive mission planning result, which may be explained by the fact that the latest cloud information is not applied, resulting in uncertainty in the scheduling process. In conclusion, the observation profit of each scenario will be effectively improved after the mission replanning, and the improvement will increase with the number of tasks.

To verify the superiority of the proposed replanning heuristic, one should compare it with other algorithms. Therefore, we introduce genetic algorithm (GA), ant colony optimization (ACO), particle swarm optimization (PSO) algorithms, and the reactive

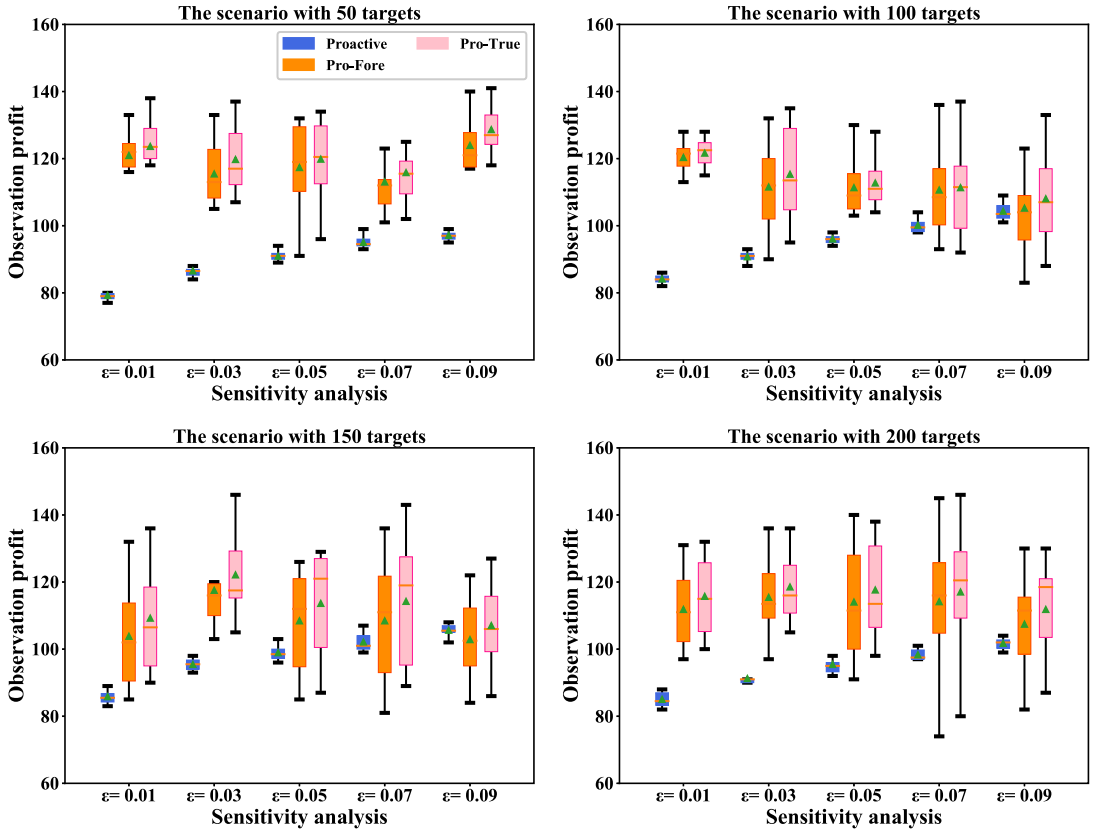

Fig. 12. Sensitivity analysis of ϵ with the different number of targets.

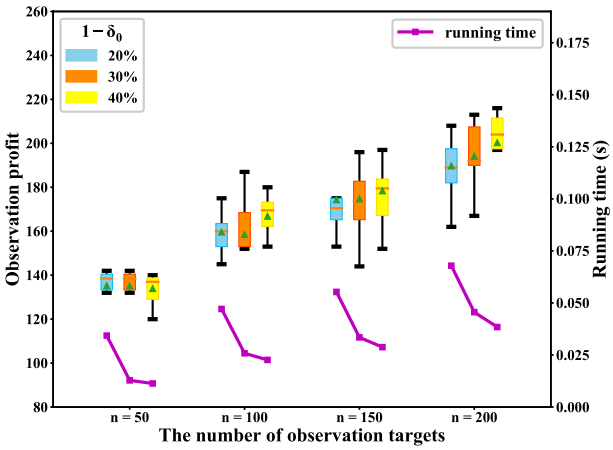

Fig. 13. Sensitivity analysis of cloud coverage threshold with the different number of targets.

scheduling algorithm (denoted as RSA) proposed in [29] to solve the problem for comparison. Standard algorithm procedures of metaheuristics have been implemented and the RSA is modified to fit the RH structure. For fairness, the same proactive mission planning results have been provided. The results of the comparative experiments are shown in Fig. 10, where the running time for each run is represented by the purple square dot. As seen from Fig. 10, the average value of the observation profit of each scenario obtained by the RHRA is higher than that of GA, ACO, PSO, and RSA. Moreover, the superiority of the RHRA becomes more obvious as the number of observation targets increases. The RSA performs better than GA, ACO, and PSO in all scenarios while consuming the least time of these four. When the number of observation targets increases from 150 to 200, the increase of the observation profit obtained by the RSA is not obvious, which indicates that the RSA performs badly in the case of a large number of targets. Overall, these results suggest that the RHRA outperforms GA, ACO, PSO, and RSA, which verifies the superiority of the proposed algorithm.

D. Comparison Results With Different Forecasting Time

Simulation experiments with different forecast times have been conducted to quantitatively evaluate the impact of the forecast horizon, which could provide a reference for the selection of the length of the forecast sequence. As shown in Fig. 11, the forecast time is set as 1, 2, and 3 h, respectively. It is apparent from this Figure that the true observation profit with the forecast time set as 3 h holds the minimum for each scenario with a different number of targets. This can be explained by the fact that the forecast accuracy would decrease as the forecast time increases, which has been detailedly explained in Section V-B. Moreover, the bottom half of the figure shows that the replanning algorithm consumes the longest computation time owing to the more RHs that need to be replanned in this situation.

Further analysis shows that the longest running time of all runs would not exceed 0.1 s, which provides significant support for the resource-constrained replanning phase. Overall, the average

observation profit difference under different forecast times is not extraordinary, and the program running time for the forecast time set as 3 h is relatively short. Considering the orbital period of the low orbit EOS and the operation of the ground control center, the forecast time of the mission replanning is chosen as 3 h in this study.

E. Sensitivity Analysis

As described in Section V-C, the observation profit of the CCP model is conservative with $\epsilon = 0.01$. The confidence level would impact the observation profit significantly, and then, we conduct the sensitivity analysis of ϵ in this section. Fig. 12 presents the experimental results with ϵ varies from 0.01 to 0.09 under a different number of targets. The Pro-Fore and Pro-True represent the observation profit of the proactive mission planning results calculated by the proposed continuous profit model under the predicted and the true cloud information, respectively. As can be seen from the figure, the difference between the CCP profit and Pro-True would generally become smaller as the value of ϵ increases. For the scenario with 50 targets, the difference becomes minimum when ϵ equals 0.07, while a similar situation achieves with ϵ set as 0.09 for the other three scenarios. Therefore, it is still difficult to determine the value of ϵ ahead of time to decrease the difference between the CCP profit and the true one, which is one of the disadvantages of the pure proactive mission planning method. Meanwhile, we can find that the average value and the distribution under Pro-Fore and Pro-True stay relatively similar in almost all scenarios, which reflects the effectiveness of cloud forecasting utilizing the latest satellite cloud images.

The cloud coverage threshold δ_0 may impact the replanning results. According to Algorithm 1, a smaller δ_0 would correspond to a larger range of task removal and update. To test the influence of δ_0 and provide more guidance for practice, the value of $1 - \delta_0$ is taken as 60%, 70%, and 80%, separately. The corresponding result is reported in Fig. 13. On average, the average observation profit with different values of $1 - \delta_0$ does not show a noticeable difference. Interestingly, the program running time decreases with the increase of the value of $1 - \delta_0$ owing to the fewer operation of task removal and task insertion. Taking the observation profit under partial cloud occlusion into account, it is reasonable to take the value of $1 - \delta_0$ as 30%.

VI. Conclusion

The AEOSs mission replanning problem based on cloud coverage forecasting is addressed in this study. As mentioned in the literature review, cloud coverage performs a serious negative influence on the Earth observation mission. The latest satellite cloud images are utilized to conduct the cloud forecasting, and the forecasting method based on deep learning and Big Data is introduced. The aim of the present research is to predict cloud information in the near future and conduct mission replanning to avoid the influence of the cloud and improve the observation profit. Relying on the forecast cloud image, a continuous observation profit model is proposed to substitute the 0–1 reward model of the CCP, which could provide a more reasonable evaluation for the images with partial cloud cover. Meanwhile, the utilization of cloud information could avoid the difficulty of the selection for the confidence parameter ϵ. A novel proactive-and-reactive mission planning framework has been constructed, where the mission replanning is operated within each RH. A replanning method RHRA combined with a rapid insertion has been proposed, which could update the mission planning result efficiently and improve the observation profit effectively. Computational results show that the cloud forecasting method is suitable for mission replanning. Besides, extensive experiments in comparison to proactive mission planning and several heuristics illustrate the effectiveness of the proposed algorithm.

This research has thrown up several questions for further investigation. The observation target in this study is point target, while the mission planning for the large area target observation remains further research, where introducing true cloud information would be very conducive to the improvement of observation profit. In addition, the application of the distributed collaborative optimization method for the AEOS mission planning problem would be usefully explored in further research.

References

[1] X. Wang, G. Wu, L. Xing, and W. Pedrycz, "Agile Earth observation satellite scheduling over 20 years: Formulations, methods and future directions," *IEEE Syst. J.*, vol. 15, no. 3, pp. 3881–3892, Sep. 2021.

[2] G. Peng *et al.*, "Solving the agile Earth observation satellite scheduling problem with time-dependent transition times," *IEEE Trans. Syst., Man, Cybern. Syst.*, to be published, doi: 10.1109/TSMC.2020.3031738.

[3] Y. Xu, X. Liu, R. He, and Y. Chen, "Multi-satellite scheduling framework and algorithm for very large area observation," *Acta Astronautica*, vol. 167, pp. 93–107, 2020.

[4] Z. Zheng, J. Guo, and E. Gill, "Onboard autonomous mission re-planning for multi-satellite system," *Acta Astronautica*, vol. 145, pp. 28–43, 2018.

[5] L. He, X. Liu, Y. Chen, L. Xing, and K. Liu, "Hierarchical scheduling for real-time agile satellite task scheduling in a dynamic environment," *Adv. Space Res.*, vol. 63, no. 2, pp. 897–912, 2019.

[6] R. Pincus, S. Platnick, S. A. Ackerman, R. S. Hemler, and R. J. P. Hofmann, "Reconciling simulated and observed views of clouds: MODIS, ISCCP, and the limits of instrument simulators," *J. Climate*, vol. 25, no. 13, pp. 4699–4720, 2012.

[7] M. D. King, S. Platnick, W. P. Menzel, S. A. Ackerman, and P. A. Hubanks, "Spatial and temporal distribution of clouds observed by MODIS onboard the terra and aqua satellites," *IEEE Trans. Geosci. Remote Sens.*, vol. 51, no. 7, pp. 3826–3852, Jul. 2013.

[8] J. Wang, X. Zhu, D. Qiu, and L. T. Yang, "Dynamic scheduling for emergency tasks on distributed imaging satellites with task merging," *IEEE Trans. Parallel Distrib. Syst.*, vol. 25, no. 9, pp. 2275–2285, Sep. 2014.

[9] J. Wang, X. Zhu, L. T. Yang, J. Zhu, and M. Ma, "Towards dynamic real-time scheduling for multiple Earth observation satellites," *J. Comput. Syst. Sci.*, vol. 81, no. 1, pp. 110–124, 2015.

[10] B. Du and S. Li, "A new multi-satellite autonomous mission allocation and planning method," *Acta Astronautica*, vol. 163, pp. 287–298, 2018.

[11] E. V. Ntagiou, C. Iacopino, N. Policella, R. Armellin, and A. Donati, "Ant-based mission planning: Two examples," in *Proc. SpaceOps Conf.*, 2018, Art. no. 2498.

[12] G. Beaumet, G. Verfaillie, and M. C. Charmeau, "Feasibility of autonomous decision making on board an agile Earth-observing satellite," *Comput. Intell.*, vol. 27, no. 1, pp. 123–139, 2011.

[13] Union of Concerned Scientists (UCS), "UCS satellite database," Accessed: Jul. 15, 2021. [Online]. Available: https://www.ucsusa.org/nuclear-weapons/space-weapons/satellite-database

[14] J. Ju and D. P. Roy, "The availability of cloud-free Landsat ETM data over the conterminous United States and globally," *Remote Sens. Environ.*, vol. 112, no. 3, pp. 1196–1211, 2008.

[15] M. He and R. He, "Research on agile imaging satellites scheduling techniques with the consideration of cloud cover," *Sci. Technol. Eng.*, vol. 13, no. 28, pp. 8373–8379, 2013.

[16] C. Han, Y. Gu, G. Wu, and X. Wang, "Simulated annealing based heuristic for multiple agile satellites scheduling under cloud coverage uncertainty," 2020, *arXiv:2003.08363*.
[17] Y. Wang, M. Long, J. Wang, Z. Gao, and P. S. Yu, "PredRNN: Recurrent neural networks for predictive learning using spatiotemporal LSTMs," in *Proc. 31st Int. Conf. Neural Inf. Process. Syst.*, 2017, pp. 879–888.
[18] X. Liu, G. Laporte, Y. Chen, and R. He, "An adaptive large neighborhood search metaheuristic for agile satellite scheduling with time-dependent transition time," *Comput. Oper. Res.*, vol. 86, pp. 41–53, 2017.
[19] M. Lemaître, G. Verfaillie, F. Jouhaud, J.-M. Lachiver, and N. Bataille, "Selecting and scheduling observations of agile satellites," *Aerosp. Sci. Technol.*, vol. 6, no. 5, pp. 367–381, 2002.
[20] G. Peng, G. Song, L. Xing, A. Gunawan, and P. Vansteenwegen, "An exact algorithm for agile Earth observation satellite scheduling with time-dependent profits," *Comput. Oper. Res.*, vol. 120, 2020, Art. no. 104946.
[21] D. Liao and Y. Yang, "Imaging order scheduling of an Earth observation satellite," *IEEE Trans. Syst., Man, Cybern., C, Appl. Rev.*, vol. 37, no. 5, pp. 794–802, Sep. 2007.
[22] J. Wang, E. Demeulemeester, X. Hu, and G. Wu, "Expectation and SAA models and algorithms for scheduling of multiple Earth observation satellites under the impact of clouds," *IEEE Syst. J.*, vol. 14, no. 4, pp. 5451–5462, Dec. 2020.
[23] J. Wang, E. Demeulemeester, and D. Qiu, "A pure proactive scheduling algorithm for multiple Earth observation satellites under uncertainties of clouds," *Comput. Oper. Res.*, vol. 74, pp. 1–13, 2016.
[24] Y. Xiao, S. Zhang, P. Yang, M. You, and J. Huang, "A two-stage flow-shop scheme for the multi-satellite observation and data-downlink scheduling problem considering weather uncertainties," *Rel. Eng. Syst. Saf.*, vol. 188, pp. 263–275, 2019.
[25] C. G. Valicka *et al.*, "Mixed-integer programming models for optimal constellation scheduling given cloud cover uncertainty," *Eur. J. Oper. Res.*, vol. 275, no. 2, pp. 431–445, 2019.
[26] J. Wang, E. Demeulemeester, X. Hu, D. Qiu, and J. Liu, "Exact and heuristic scheduling algorithms for multiple Earth observation satellites under uncertainties of clouds," *IEEE Syst. J.*, vol. 13, no. 3, pp. 3556–3567, Sep. 2019.
[27] X. Wang, G. Song, R. Leus, and C. Han, "Robust Earth observation satellite scheduling with uncertainty of cloud coverage," *IEEE Trans. Aerosp. Electron. Syst.*, vol. 56, no. 3, pp. 2450–2461, Jun. 2020.
[28] X. Wang, Y. Gu, G. Wu, and J. R. Woodward, "Robust scheduling for multiple agile Earth observation satellites under cloud coverage uncertainty," *Comput. Ind. Eng.*, vol. 156, 2021, Art. no. 107292.
[29] J. Wang, X. Hu, and C. He, "Reactive scheduling of multiple EOSs under cloud uncertainties: Model and algorithms," *J. Syst. Eng. Electron.*, vol. 32, no. 1, pp. 163–177, 2021.
[30] F. Kurzrock *et al.*, "A review of the use of geostationary satellite observations in regional-scale models for short-term cloud forecasting," *Meteorologische Zeitschrift*, vol. 27, no. 4, pp. 277–298, 2018.
[31] G. Roussel, O. Liandrat, S. Cros, M. Turpin, and S. Rainjonneau, "Qualification of a new short-term cloud forecasting method for the optimization of Earth observation satellite programs," *Proc SPIE*, vol. 10786, 2018, Art. no. 107860P.
[32] S. Cros, N. Sébastien, O. Liandrat, and N. Schmutz, "Cloud pattern prediction from geostationary meteorological satellite images for solar energy forecasting," *Proc. SPIE*, vol. 9242, 2014, Art. no. 924202.
[33] D. Dissawa, M. Ekanayake, G. Godaliyadda, J. B. Ekanayake, and A. P. Agalgaonkar, "Cloud motion tracking for short-term on-site cloud coverage prediction," in *Proc. 17th Int. Conf. Adv. ICT Emerg. Regions*, 2017, pp. 1–6.
[34] M. Penteliuc and M. Frincu, "Prediction of cloud movement from satellite images using neural networks," in *Proc. 21st Int. Symp. Symbolic Numeric Algorithms Sci. Comput.*, 2019, pp. 222–229.
[35] X. Shi *et al.*, "Deep learning for precipitation nowcasting: A benchmark and a new model," in *Proc. Conf. Neural Inf. Process. Syst.*, 2017, pp. 5617–5627.
[36] X. Shi, Z. Chen, H. Wang, D. Y. Yeung, W. K. Wong, and W. C. Woo, "Convolutional LSTM network: A machine learning approach for precipitation nowcasting," in *Proc. Adv. Neural Inf. Process. Syst.*, 2015, vol. 2015, pp. 802–810.
[37] G. Roussel, M. Turpin, Y. Bardout, and G. Jubelin, "Adaptation of short-term cloud forecasting to global scale and evaluation of its contribution to Earth observing satellite planning," *IEEE J. Sel. Topics Appl. Earth Observ. Remote Sens.*, to be published, doi: 10.1109/JSTARS.2021.3126451.
[38] S. Oprea *et al.*, "A review on deep learning techniques for video prediction," *IEEE Trans. Pattern Anal. Mach. Intell.*, to be published, doi: 10.1109/TPAMI.2020.3045007.
[39] J. Luedtke and S. Ahmed, "A sample approximation approach for optimization with probabilistic constraints," *SIAM J. Optim.*, vol. 19, no. 2, pp. 674–699, 2008.
[40] N. Metropolis and S. Ulam, "The Monte Carlo method," *J. Amer. Stat. Assoc.*, vol. 44, no. 247, pp. 335–341, 1949.
[41] National Satellite Meteorological Center (NSMC), "FY-2 satellite cloud image," Accessed: Sep. 1, 2020. [Online]. Available: http://www.nsmc.org.cn/NewSite/NSMC/Channels/100028.html
[42] S. Sural, G. Qian, and S. Pramanik, "Segmentation and histogram generation using the HSV color space for image retrieval," in *Proc. Int. Conf. Image Process.*, 2002, vol. 2, pp. II–II.
[43] C. Han, X. Wang, G. Song, and R. Leus, "Scheduling multiple agile Earth observation satellites," FEB Res. Rep. KBI_1813, 2018.
[44] Y. Liang, J. Sun, H. Li, Y. Zhou, R. Zhang, and S. Li, "Single-layer cloud base height estimation based on ISCCP cloud-type classification and weighted distance (in Chinese)," *Meteorological*, vol. 43, no. 10, pp. 1224–1231, 2017.
[45] L. He, X. Liu, G. Laporte, Y. Chen, and Y. Chen, "An improved adaptive large neighborhood search algorithm for multiple agile satellites scheduling," *Comput. Oper. Res.*, vol. 100, pp. 12–25, 2018.
[46] G. Peng, R. Dewil, C. Verbeeck, A. Gunawan, L. Xing, and P. Vansteenwegen, "Agile Earth observation satellite scheduling: An orienteering problem with time-dependent profits and travel times," *Comput. Oper. Res.*, vol. 111, pp. 84–98, 2019.
[47] A. Paszke *et al.*, "PyTorch: An imperative style, high-performance deep learning library," in *Proc. Adv. Neural Inf. Process. Syst.*, 2019, vol. 32, pp. 8026–8037.
[48] Z. Wang, A. C. Bovik, H. R. Sheikh, and E. P. Simoncelli, "Image quality assessment: From error visibility to structural similarity," *IEEE Trans. Image Process.*, vol. 13, no. 4, pp. 600–612, Apr. 2004.

Yi Gu received the B.S. degree in aerospace engineering, in 2017, from Beihang University, Beijing, China, where he is currently working toward the Ph.D. degree.

His research interests include satellite mission planning and intelligent optimization methods.

Chao Han was born in Beijing, China, in 1960. He received the M.S. and Ph.D. degrees in applied mechanics from Beihang University, Beijing, in 1985 and 1989, respectively.

He is currently a Professor with the School of Astronautics, Beihang University. His research interests include the area of spacecraft orbit and attitude dynamics, spacecraft guidance, navigation, and control.

Yuhan Chen received the B.S. degree in aerospace engineering, in 2019, from Beihang University, Beijing, China, where he is currently working toward the master degree in aerospace science and technology.

His research interests include mission planning and simulation technology.

Wei W. Xing received the Ph.D. degree in engineering from the University of Warwick, Coventry, U.K., in 2017.

He worked as a Postdoc Fellow with the Scientific Computing Institute (SCI), University of Utah, Salt Lake City, UT, USA, until 2020. He is currently an Assistant Professor with Beihang University, Beijing, China. His research interests include machine learning for scientific computing, including surrogate models, Bayesian optimization, inverse problems, digital twins, and uncertainty quantification.